Selective Activation of the Thyroid Hormone Receptor Beta (TRβ) Induces Tumor Suppression and Increases Efficacy of Therapeutic Agents

Noelle Gillis, PhD[1,2,3], Lauren Cozzens, BS[1,4], Emily Wilson, BS[1,5], Cole Davidson, PhD[1,2,6], Jennifer Tomczak, MPH[1], Eric Bolf, PhD[1,2,7], Frances Carr, PhD[1,2**]

[1] *Department of Pharmacology, Larner College of Medicine, Burlington, Vermont*

[2] *University of Vermont Cancer Center, Burlington, Vermont*

[3] *Current address: Masonic Cancer Center, University of Minnesota, Minneapolis, Minnesota*

[4] *Current address: University of Colorado, Anschutz Medical Campus, Aurora, Colorado*

[5] *Current address: University of Utah, Salt Lake City, Utah*

[6] *Current address: Wartburg College, Waverly, Iowa*

[7] *Current address: 2seventy Bio, Cambridge Massachusetts*

[**] *Corresponding author,* Email: frances.carr@med.uvm.edu

Short title: TRβ agonist blunts tumor progression and enhances therapies

Keywords: GC-1, Sobetirome, thyroid hormone receptor, anaplastic thyroid cancer

Noelle Gillis, gilli431@umn.edu; University of Minnesota, Minneapolis MN, 55455

Lauren Cozzens, lauren.cozzens@cuanschutz.edu; University of Colorado at Anschutz, Aurora, CO 80045

Emily Wilson, u1414297@utah.edu, University of Utah, Salt Lake City, UT 84116

Cole Davidson, cole.davidson@wartburg.edu, Wartburg College, Waverly IA 50677

Jennifer Tomczack, jennifer.tomczak@uvm.edu; University of Vermont College of Medicine, Pharmacology, Burlington, VT, 05405 USA; 802-656-9617

Eric Bolf, eric.bolf@2seventybio.com Cambridge MA 02142

Frances Carr, frances.carr@med.uvm.edu; University of Vermont College of Medicine, Pharmacology, Burlington, VT, 05405 USA; 802-656-6318

The authors declare no potential conflicts of interest.

Abstract

Thyroid hormone receptor beta (TRβ) is a recognized tumor suppressor in numerous solid cancers. The molecular signaling of TRβ has been elucidated in several cancer types through re-expression models. Remarkably, the potential impact of selective activation of endogenous TRβ tumor progression remains largely unexplored. We used cell-based and *in vivo* assays to evaluate the effects of the TRβ agonist sobetirome (GC-1) on a particularly aggressive and dedifferentiated cancer, anaplastic thyroid cancer (ATC). Here we report that GC-1 reduced tumorigenic phenotypes, decreased cancer stem-like cell population, and increased the efficacy of current therapeutics. GC-1 induced re-differentiation of the ATC cells and increased sodium-iodide transporter (NIS) expression and restored iodide uptake. GC-1 alone was as effective as Sorafenib in blunting tumor growth *in vivo*. These results indicate that selective activation of TRβ not only induces a tumor suppression program *de novo* but enhances the effectiveness of anti-cancer agents.

Statement of Significance: Selective activation of TRβ reduces aggressive cancer cell phenotype, cancer stem cell population, tumor growth and increases the efficacy of current therapeutics. TRβ is a novel diagnostic biomarker and therapeutic target.

57 **INTRODUCTION**

58 There is compelling evidence that the nuclear receptor thyroid hormone receptor
59 beta (TRβ) is a suppressor of tumor progression, invasion, and metastases in multiple
60 solid tumors including thyroid, breast, colon and other cancers(1). Cell-based and animal
61 studies reveal that liganded TRβ induces apoptosis, reduces an aggressive phenotype,
62 decreases cancer stem cell populations, and slows tumor growth through modulation of
63 a complex transcriptional network (2-9) . Transcriptional regulation by TRβ is critical for
64 its function as a tumor suppressor because it acts as both a signal transducer and
65 facilitator of long-term epigenetic programming for maintenance of cell identity. Our recent
66 studies revealed that TRβ in the presence of triiodothyronine (T_3) induced a tumor-
67 suppressive transcriptomic program and cell redifferentiation in aggressive thyroid and
68 breast cancer cells (2,10). We identified several key mechanisms by which activation of
69 TRβ could reduce tumor progression, implicating thyroid hormone signaling as a
70 therapeutic opportunity in advanced cancers. Recent studies in breast (8), colon (11), and
71 liver (5) cancers also emphasize this untapped therapeutic potential (12,13).

72 Thyroid hormones, thyromimetics and their metabolites can activate TRα as well
73 as TRβ. Yet, the use of non-selective TRβ ligands, such as T_3, is problematic as a
74 therapeutic approach due to the adverse side-effects of hyperthyroidism and the potential
75 for cardiovascular events as a result of aberrant TRα activity. To subvert these negative
76 side effects, TRβ-selective thyromimetics have been developed (14,15). Several of these
77 drugs have been shown to be effective for treatment of metabolic and neurodegenerative
78 disorders in clinical trials(15). In particular, the TRβ agonist sobetirome (GC-1)

79 preferentially binds to and activates TRβ and induces the same transcriptomic response
80 as T_3 (15, 16) and has been successful in early clinical trials for treatment of dyslipidemia
81 (16-19). Despite their potential benefits demonstrated by numerous preclinical studies,
82 TRβ agonists remain untested as cancer therapeutics as single agents or in combination
83 with other treatments.

84 Here, we investigated the potential impact of a selective TRβ agonist in an
85 aggressive thyroid cancer model. The global incidence of thyroid cancer is increasing
86 faster than any other solid tumor (20,21). While prognoses for patients with differentiated
87 tumors receiving standard therapies are generally very good, outcomes for patients with
88 resistant or recurrent disease and poorly differentiated thyroid cancers (PDTC) are
89 extremely poor (22). Due to a lack of effective therapies, patients with advanced or
90 metastatic anaplastic thyroid cancer (ATC) have a higher mortality rate than all other
91 endocrine cancers combined (23). ATC tumors are refractory to radioiodine therapy due
92 to loss of the sodium-iodide symporter (NIS) expression, and traditional chemotherapy is
93 of limited benefit.

94 Activation of phosphatidylinositol 3-kinase (PI3K)–Akt–mammalian target of
95 rapamycin (mTOR) pathway (PI3K-Akt) and mitogen-activated protein kinase (MAPK)
96 signaling are recognized drivers of thyroid oncogenesis and blocking this activity is a
97 therapeutic focus. Yet inhibitors of the major components of these signaling cascades
98 rarely provide a durable response as resistance quickly develops. Current molecular
99 diagnostics provide a rationale for intervention with combination therapies (24). However,
100 combination treatments have not yielded significantly improved responses due to

101 development of resistance, and there are still no curative options (14). Therefore, there
102 remains an urgent need for innovative and less toxic therapeutics for ATC (25-27).

103 In our studies we establish the effects of GC-1 alone and in combination with
104 therapeutic agents in ATC cells with diverse genetic backgrounds (28). GC-1 alone
105 decreases the aggressive phenotype and increases the effectiveness of MAPK, PI3K,
106 and cell cycle inhibitors. GC-1 significantly increases expression of thyroid-specific genes,
107 inducing re-differentiation in ATC cells. Importantly, we observe an increase in NIS protein
108 which leads to enhanced iodide uptake implicating potential restoration of functionality.
109 Finally, GC-1 alone reduced tumor growth of ATC cells in xenografts as effectively as
110 Sorafenib. The combination of GC-1 and Sorafenib maximally suppressed tumor growth.
111 These observations indicate that activation of TRβ with isomer-selective agonists may be
112 an effective and practical adjuvant therapeutic strategy.

113 **RESULTS**

114 **GC-1 blocks the tumorigenic phenotype of ATC cells transduced with TRβ.**

115 We previously demonstrated that T_3 (10 nM) treatment of transduced SW1736
116 cells, in which TRβ is re-expressed (SW-TRβ), induced a tumor suppression
117 transcriptomic program and reduced cell growth when compared to cells transduced with
118 empty vector (SW-EV) (2). We therefore tested the ability of GC-1 (10 nM) to reduce ATC
119 phenotypes. We found that GC-1 similarly decreased cell growth in four days (**Fig. 1A**).
120 There was a 50% reduction in the overall growth rate of SW-EV cells and 75% reduction
121 in SW-TRβ cells (**Fig. 1B**), indicating potent activation of endogenous TRβ. There was
122 also a modest decrease in the cell migration rate of upon treatment with GC-1 (**Fig. 1C**).

As cancer stem cells are thought to be responsible for tumor initiation and recurrence, targeting these cells is key to successful treatment. Therefore, we tested whether thyroid cancer stem cells are responsive to GC-1. Thyrosphere formation is robust in SW-EV cells, and GC-1 induced a significant reduction in growth (**Fig. 1D**). Re-expression of TRβ (SW-TRβ) reduces thyrosphere growth and addition of GC-1 reduces thyrosphere formation by approximately 80% (**Fig. 1D**). These results indicate that GC-1 can activate TRβ to reduce the thyroid cancer stem cell population.

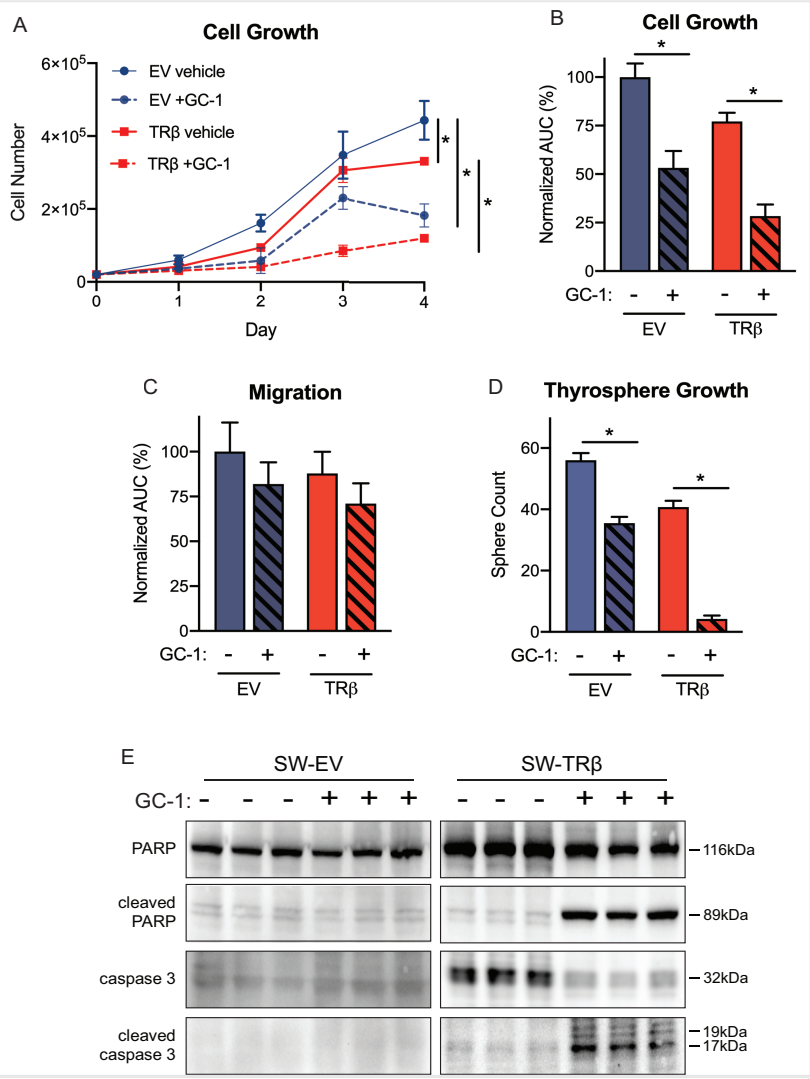

Figure 1. GC-1 blocks tumorigenic phenotypes in ATC cells transduced with TRβ. A. Growth curves demonstrate that SW-TRβ growth is significantly decreased after treatment with GC-1 for 4 days (n=3). Significance (* $p<0.05$) was determined by a two-way ANOVA and Tukey's multiple comparisons test. **B**. Area under the curve (AUC) analysis of growth curve data. Significance (* $p<0.05$) was determined by t-test. **C.** Treatment with GC-1 slows migration of SW-TRβ and SW-EV cells measured by scratch assay. Significance (* $p<0.05$) was determined by t-test. D. GC-1 repressed thyrosphere formation in SW-TRβ and SW-EV cells (n=4). Significance (* $p<0.05$) was determined by t-test. E. Immunoblot demonstrates that 5 days of GC-1 treatment induces apoptosis in SW-TRβ cells assessed by cleavage of PARP and caspase 3 (n=3).

146 Apoptotic signaling is central to ligand-activated TRβ modulation of the ATC
147 aggressive phenotype (2). Thus, we assessed the effects of GC-1 on PARP and caspase
148 3 cleavage by immunoblot as markers of late-stage apoptosis (**Fig. 1E**). GC-1 significantly
149 increased cleavage of PARP and caspase 3 in SW-TRβ consonant with increased
150 apoptotic signaling. Combined, these results indicate that GC-1 can activate TRβ to
151 reduce the aggressive phenotype in transduced ATC cells with TRβ re-expressed and
152 recapitulate effects seen with T_3 at comparable concentrations.

153 **GC-1 slows growth of parental ATC cells.**

154 Once we confirmed that GC-1 induces the same phenotypic changes in our
155 transduced ATC cell line model, it was critical to assess whether selective activation of
156 endogenous TRβ would induce similar effects in unmodified ATC cell lines (28). SW1736,
157 8505C, OCUT2, and KTC-2 cells all harbor *BRAF*^{V600E} and *TERT* driver mutations, but
158 otherwise have diverse mutational backgrounds (summarized in **Fig. 2A**). Endogenous
159 TRβ expression is low in all four ATC cell lines when compared with normal thyroid cells
160 (29). Treatment of each cell line with 10 nM GC-1 for four days yielded a modest but
161 significant decrease in cell growth (**Fig. 2B-E**). Treatment with 10 nM T_3 did not alter
162 growth of any of the cell lines. This result suggests that even low levels of endogenous
163 TRβ can be selectively activated with GC-1, and GC-1 is more effective at promoting
164 tumor suppressor activity than T_3.

165

A

Gene Function	Gene Name	Cell Line: SW1736	8505C	OCUT-2	KTC-2
		Mutation Type			
MAPK Signaling	BRAF	V600E	V600E	V600E	V600E
Telomerase	TERT (promoter)	124C-T	146C-T	146C-T	124C-T
DNA Homeostasis	TP53	Trunc.	Miss.		
PI3K Signaling	PIK3CA			Kinase Domain	
Cell-Cell Contact	NF2		Trunc.		
DNA Homeostasis	ATM		Trunc.		
TSH Signaling	TSHR	Miss.			
Histone Methyltransferase	KMT2C				Miss.
Histone Methyltransferase	KMT2D				Trunc.
Histone Acetyltransferase	EP300	Trunc.			
SWI/SNF Complex	ARID1A				In Frame
SWI/SNF Complex	SMARCA4		Miss.		

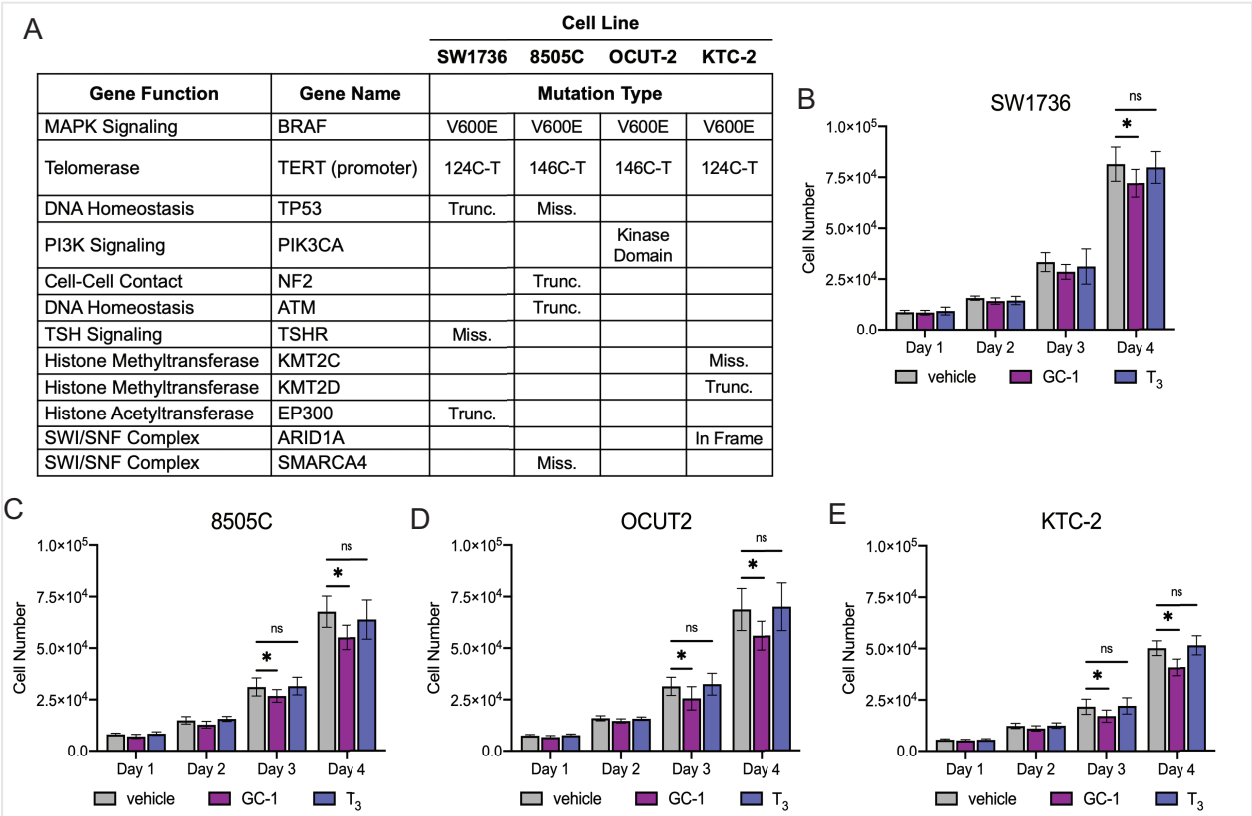

Figure 2: GC-1 slows growth of parental ATC cells. A. Summary of mutated genes in four ATC cell lines implemented in this study (17). B-E. Relative cell growth of unmodified ATC cell lines was measured by cell counting assay after 4 days of treatment with 10 nM GC-1 or 10 nM T_3. Significance (* $p<0.05$) was determined by a two-way ANOVA followed by Dunnett's multiple comparisons test; 3 independent experiments were performed per treatment group.

GC-1 increases the efficacy of selected therapeutic agents

Based on our previous work on activation of TRβ in ATC cells, we hypothesized that GC-1 could enhance the efficacy of therapeutics that target selective pathways. Cell viability was calculated following treatment for three days with increasing concentrations of the PI3K inhibitor Buparlisib (pan-PI3K inhibitor) or Alpelisib (PI3Kα mutant inhibitor) for OCUT2 cells which harbor a gain-of-function *PIK3CA* mutation (**Fig. 3A**), the cell cycle inhibitor Palbociclib (**Fig. 3B**), or the multi-tyrosine kinase inhibitor Sorafenib (**Fig. 3C**), with or without 10 nM GC-1. Each therapeutic agent decreased cell viability in three days

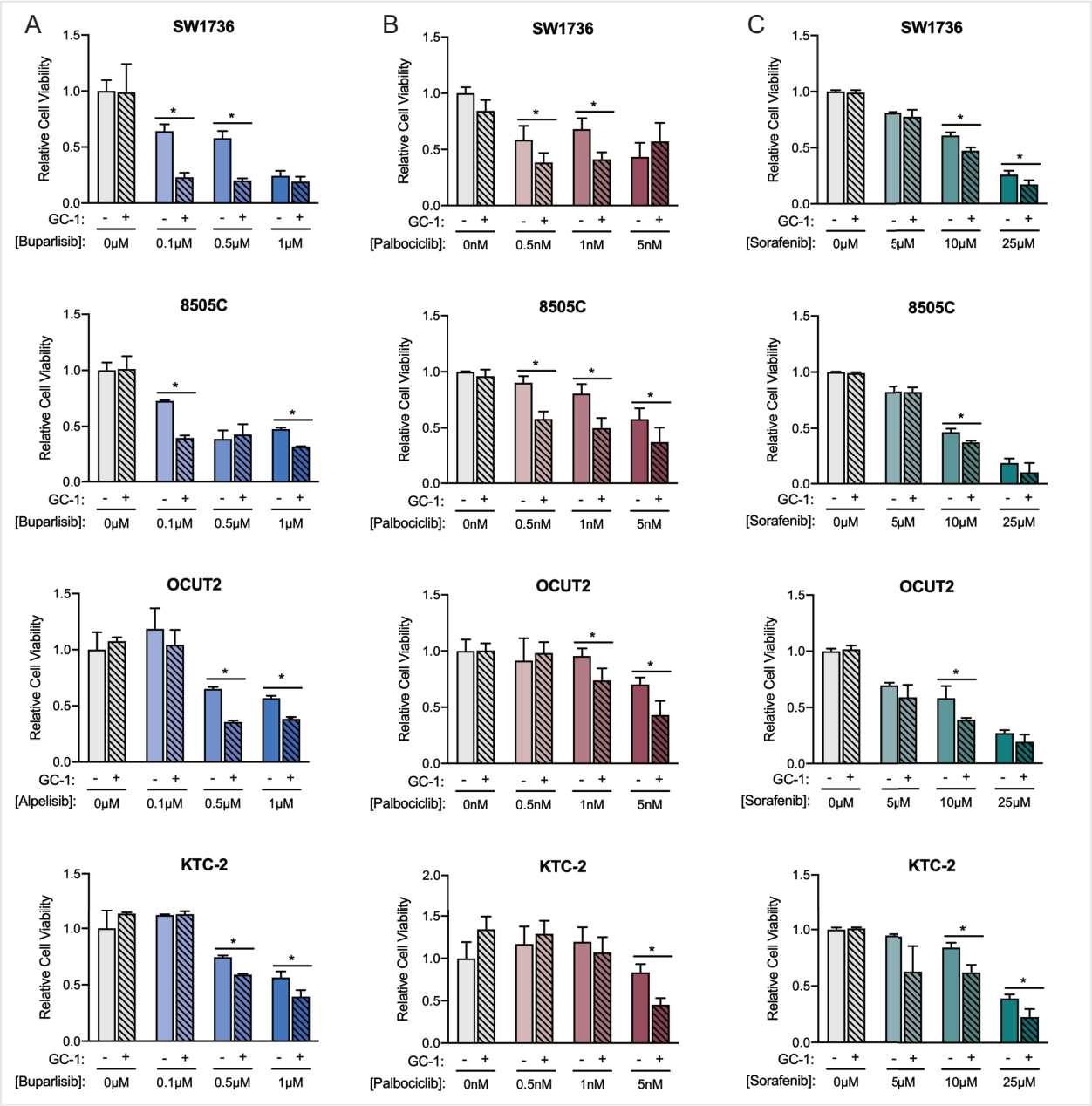

Figure 3. GC-1 increases efficacy of inhibitors. Cell viability of unmodified ATC cell lines was measured by SRB assay after 3 days of treatment with increasing concentrations buparlisib or alpelisib (A), sorafenib (B), or palbociclib (C) simultaneously in combination with 10 nM GC-1. Significance (* $p<0.05$) was determined by a two-way ANOVA followed by Sidak's multiple comparisons test; 3 independent experiments were performed per each treatment group.

174 in a dose-dependent manner. The addition of GC-1 significantly increased the efficacy of

175 these agents at lower concentrations. For example, 1 μM Buparlisib was required to

176 reduce cell viability below 50% in the absence of GC-1, but when combined with 10 nM
177 GC-1 this could be achieved with 0.1-0.5 μM Buparlisib (**Fig. 3A**). Similar trends were
178 observed with all four therapeutics and across the panel of cell lines used.

179 **GC-1 enhances the effects of therapeutic agents on cell migration**

180 In addition to reducing cell viability, many therapeutics target pathways that are
181 involved in cell migration. To further evaluate the ability of GC-1 to enhance the efficacy
182 of select therapeutics, cells were treated with the indicated inhibitors at concentrations
183 determined to be effective based on cell viability assays (**Fig. 3**), and migration was
184 observed by assessing wound closure. Each inhibitor was able to successfully slow
185 migration, and this effect was increased when each of the inhibitors were combined with
186 GC-1, except for Buparlisib in KTC-2 cells (**Fig. 4B-E**). Notably, GC-1 alone was able to
187 prevent wound closure of all cell lines with similar success as each inhibitor alone (**Fig.**
188 **4A-E**). These findings are similar to what we previously observed in experiments using
189 endogenous thyroid hormone, T_3, indicating GC-1 is a suitable alternative for TRβ
190 activation for slowing migration.

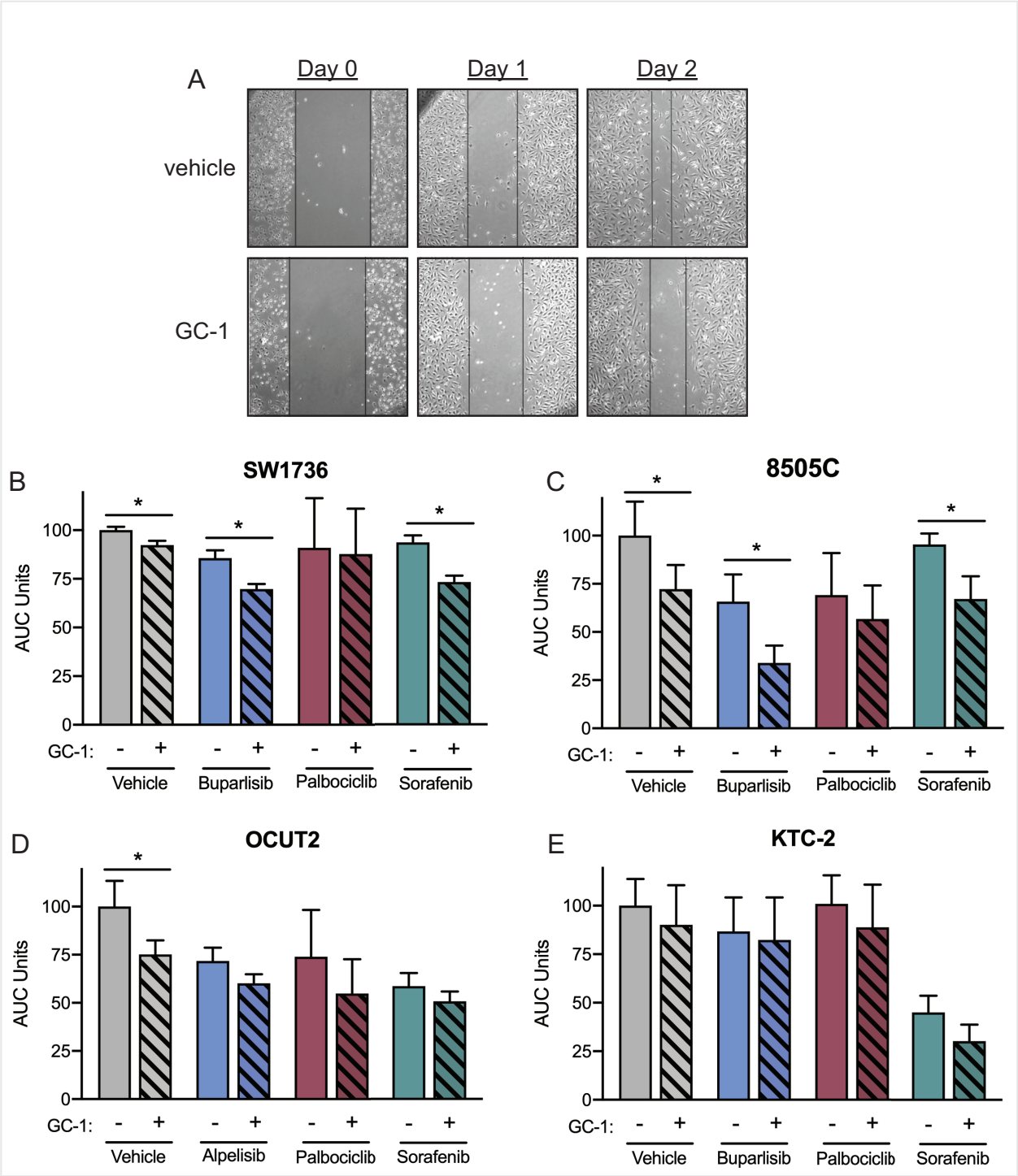

Figure 4. GC-1 enhances the effects of inhibitors on cell migration. Cell migration was measured by scratch assay. Representative images demonstrate reduced scratch closure after two days when ATC cells are treated with GC-1 (A). Area under the curve (AUC) analysis shows SW1736 (B), 8505C (C), OCUT2 (D), and KTC-2 (E) cells all exhibit lower rates of scratch closer after treatment with GC-1 alone and further reduced scratch closure rates after combined treatment with GC-1 and inhibitors. Significance (* $p<0.05$) was determined by t-test.

192 **GC-1 blocks tumorsphere outgrowth and increases efficacy of therapeutic agents.**

193 Current treatment options for ATC primarily target hyperproliferative cells, but
194 aggressive cancers like ATC are enriched for long-lived cancer stem cells that are thought
195 to be a major mechanism for therapy resistance and tumor recurrence. We previously
196 demonstrated that ligand-activated TRβ regulates genes related to stemness in ATC cells
197 and that GC-1 could block thyrosphere outgrowth in our modified ATC cells (**Fig. 1D**). We
198 therefore tested the hypothesis that GC-1 could prevent thyrosphere outgrowth after an
199 initial treatment with an inhibitor that targets proliferation.

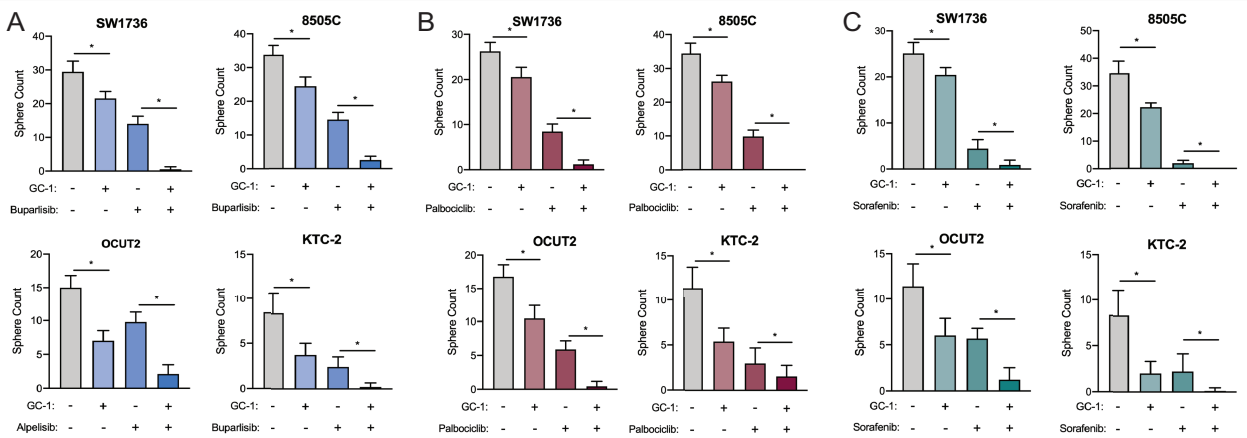

Figure 5. GC-1 blocks thyrosphere outgrowth and increases the efficacy of therapeutic agents. Thyrosphere growth was determined for ATC cells after 3 days of treatment with 0.5 μM buparlisib or alpelisib (A), 10 μM sorafenib (B), or 1 nM palbociclib (C) under adherent culture conditions, followed by plating in conditions for spheroid growth in the presence of 10 nM GC-1 for 7 days. GC-1 alone and each therapeutic agent significantly blocked sphere formation in all cell types. GC-1 in addition to each therapeutic agent further inhibited or completely blocked sphere formation. Significance (* $p<0.05$) was determined by two-way ANOVA followed by Sidak's multiple comparisons test; 3 independent experiments were performed per each treatment group; n=3 per analyses.

200 ATC cells were treated with the indicated inhibitor or vehicle for three days,
201 followed by re-plating in non-adherent conditions. We again observed that GC-1 alone
202 could reduce thyrosphere formation in unmodified ATC cell lines (**Fig. 5A-C**). None of the
203 inhibitors could completely prevent thyrosphere outgrowth when used alone; however,
204 Sorafenib was the most effective overall (**Fig. 5C**). The addition of GC-1 upon removal of

205 each inhibitor blocked nearly all thyrosphere outgrowth. This effect was consistent across
206 all four cell lines and all three inhibitors used. This suggests that GC-1 may be particularly
207 effective at blocking cancer stem cell expansion.

208 **GC-1 promotes re-differentiation of ATC cell lines.**

209 In transduced cells, TRβ activation with T_3 reduces the aggressive phenotype
210 partially through re-differentiation. Therefore, we investigated the potential for GC-1 to
211 promote re-differentiation in parental SW1736 cells. Gene expression analysis using RT-
212 qPCR revealed that 24 hours of GC-1 exposure increased levels of thyroid-specific gene
213 transcripts (**Fig. 6A**). This transcriptomic program is summarized by the thyroid
214 differentiation score (TDS), which significantly increased in GC-1-treated cells (**Fig. 6B**).
215 Additionally, GC-1 alone decreased the overall number of $CD24^-/CD44^+$ cells present in
216 the monolayer population as evident by RT-qPCR (**Sup. Fig. 1A**). We also observed a
217 decrease in the ATC markers *ALCAM* (CD166) and *ALDH1A1* (**Sup. Fig. 1B**).

218 Intriguingly, *SLC5A5* expression was increased with 24 hours of GC-1 (**Fig. 6A**).
219 Therefore, we further investigated NIS protein levels after 48 hours of GC-1 treatment.
220 Both nascent and mature (glycosylated) NIS protein significantly increased following GC-
221 1 treatment (**Fig. 6C-D**). Iodide uptake into cells also increased (**Fig. 6E**), indicating that
222 the increased NIS protein was functional. These findings reveal a novel function of GC-1

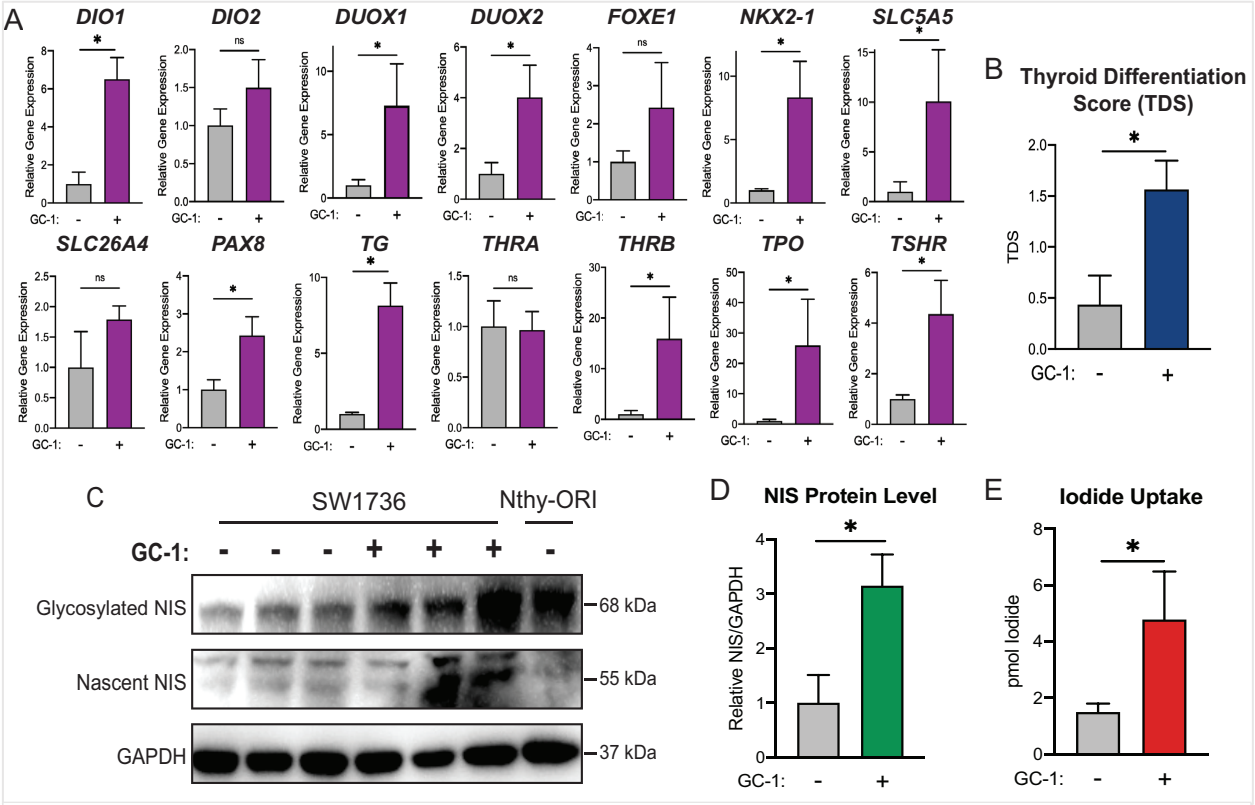

Figure 6. GC-1 induces expression of redifferentiation markers in SW1736 cells. A. RT-qPCR for thyroid differentiation markers was performed on SW1736 cells treated with or without 10 nM GC-1 for 24 hours. mRNA levels in cells treated with GC-1 are relative to the untreated cells. Significance (* $p<0.05$) was determined by Student's unpaired t test; 3 independent experiments were performed per treatment group. B. Thyroid differentiation score (TDS) was calculated using the expression level of the genes in panel A, excluding *THRB*, as previously described (10, 17). Significance (* $p<0.0001$) was determined by Student's unpaired t test. C. SW1736 cells were treated with or without 10 nM GC-1 in triplicate for 48 hours prior to protein extraction and analysis via immunoblot. Normal-like thyroid Nthy-ORI cells were used as a positive control. D. Relative NIS/GAPDH protein levels from (C) were quantified via ImageJ, and significance (* $p<0.01$) was determined by Student's unpaired t test. E. Iodide uptake was measured after 48 hours of GC-1 treatment. Significance was determined by Student's unpaired t test. (* $p<0.001$).

223 to induce re-differentiation in an ATC cell line model and offers a promising target to
224 increase NIS levels and iodide uptake.

225 **GC-1 blunts tumor growth as effectively as Sorafenib *in vivo.***

226 To validate our cell-based findings *in vivo*, the effect of GC-1 alone or in
227 combination with Sorafenib was tested in a xenograft study. GC-1 blunted tumor growth
228 with no significant change in tumor volume over the treatment period similar to Sorafenib
229 and the combination of both treatments (Fig. 7A). At day 16 of treatment, GC-1 induced
230 a significant 60% reduction in tumor mass as did Sorafenib (Fig. 7B, C). The potential for
231 drug synergy was masked due to the equivalent efficacy with Sorafenib at these doses
232 (7A-C). Of note, All mouse groups exhibited similar weight gains over the course of
233 treatment (Fig. 7D). Immunofluorescence image analysis (HALO) on excised tumors
234 revealed diminished Ki67 in all treatment groups (Fig. 7E-F). The combination of GC-1
235 and Sorafenib resulted in a significant reduction in Ki67 expression (Fig. 7F). Region of
236 Interest (ROI) analysis revealed distribution of Ki67 expression preferential in cells along
237 the periphery of the tumor samples.

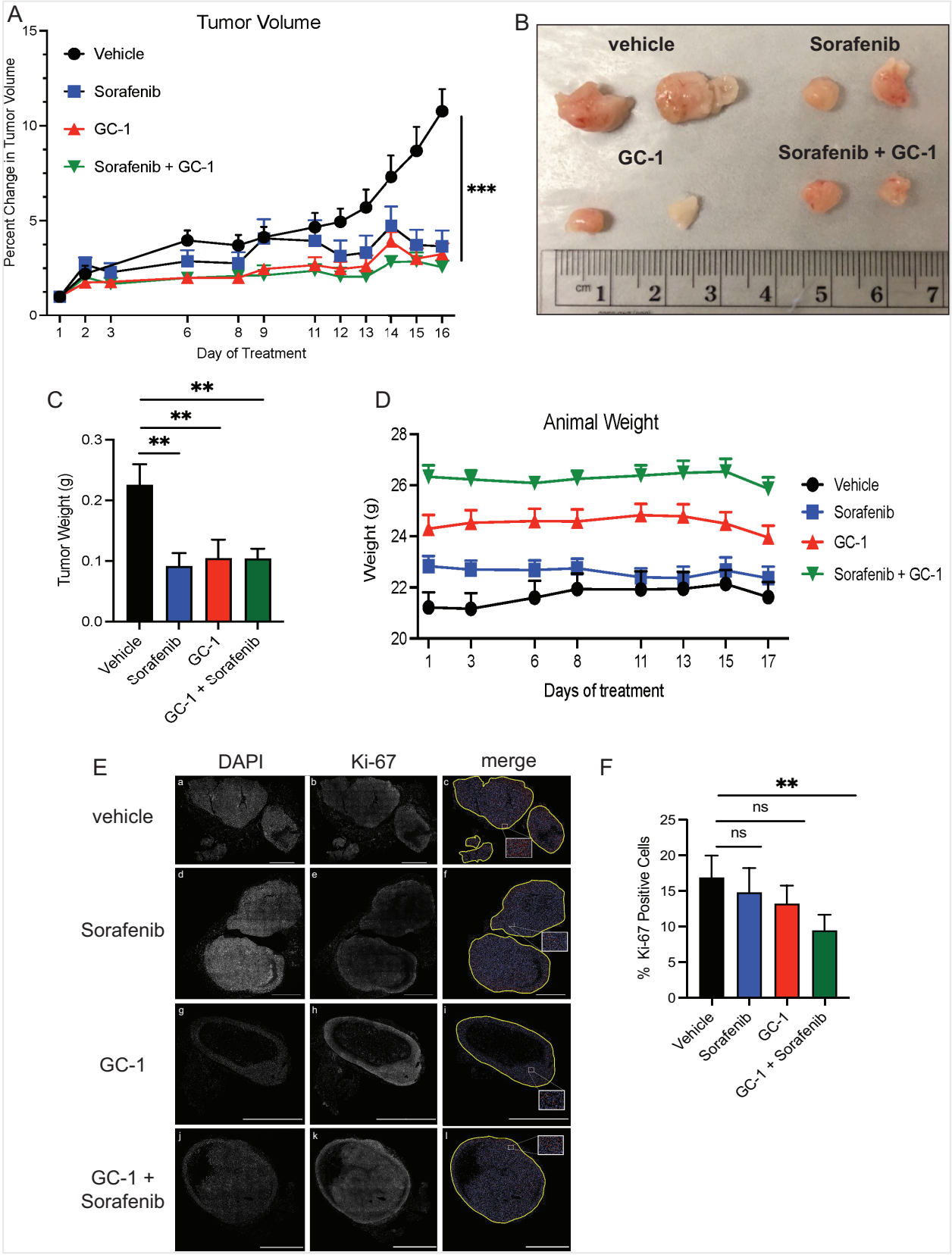
A
Tumor Volume
Vehicle
Sorafenib
GC-1
Sorafenib + GC-1
Percent Change in Tumor Volume
Day of Treatment
***
B
vehicle
Sorafenib
GC-1
Sorafenib + GC-1
C
Tumor Weight (g)
Vehicle
Sorafenib
GC-1
GC-1 + Sorafenib
D
Animal Weight
Weight (g)
Days of treatment
Vehicle
Sorafenib
GC-1
Sorafenib + GC-1
E
DAPI
Ki-67
merge
vehicle
Sorafenib
GC-1
GC-1 + Sorafenib
F
% Ki-67 Positive Cells
ns
Vehicle
Sorafenib
GC-1
GC-1 + Sorafenib

Figure 7. GC-1 inhibits tumor growth as effectively as Sorafenib in an ATC xenograft model. Nude mice were injected subcutaneously with 1 x 10^6 8505C cells. Tumors were established after 1 week. Mice were assigned to 4 treatment groups by weight and injected i.p. daily for 16 days with vehicle control, 10 mg/kg sorafenib, 0.3 mg/kg GC-1, or a combination of sorafenib and CP. (A) Percent change in tumor volumes from day 1 of treatment; *** $p<0.001$ (B) Representative excised tumors from each treatment. No evidence of metastases was noted in any group. Reduced vascularization was observed with GC-1 treatment. (C) Tumors were excised on Day 16 and weighed. Sorafenib (blue), GC-1 (red) induced a 60% reduction in final tumor mass with no difference between the two treatments. The combined treatments did not further reduce the tumor mass over the time period. Significance indicated ** $p<0.01$. (D) Mice were weighed three times a week following drug injections to monitor toxicity. No significant change in animal weight was noted for any group. (E) Representative images of tumors stained for Ki-67 are illustrated. Regions of interest containing only tumor tissue were outlined on each tiled image. Nuclear detection was set to the DAPI channel and the nuclear detection settings were optimized to accurately segment nuclei in the images. (F) Images were analyzed using HALO image analysis (Indica Labs, Albuquerque NM; version 3.3.45) utilizing the HighPlex FL module (version 4.1.3). Quantification of Ki-67 fluorescent intensity per cell is summarized. Sorafenib and GC-1 decreased Ki-67 but only significantly in combination; **$p<0.01$.

DISCUSSION

There is compelling evidence that loss of expression of TRβ, a member of the thyroid hormone receptor (TR) family, through genomic modifications and epigenetic silencing is characteristic of thyroid tumors (3,30-35). Numerous pre-clinical studies demonstrate the potent anti-tumorigenic effect of robust expression of the *THRB* gene. Re-expression of silenced TRβ using demethylating agents delays thyroid tumor progression *in vivo* (36), mice expressing a c-terminal frameshift of TRβ ($Thrb^{PV}$) spontaneously develop follicular thyroid cancer (37), and $Thrb^{PV/PV}$ $Kras^{G12D}$ mice develop thyroid tumors with features of de-differentiated thyroid cancer (38). Our studies in anaplastic thyroid cancer cells revealed that activation of TRβ induces a tumor suppression transcriptomic program, re-differentiation, and reduces the aggressive phenotype (2,10).

Activation of TRβ in pre-clinical and clinical studies have yielded exciting results

252 with great promise for novel interventions. Patients who were rendered hypothyroxinemic
253 and treated with T_3 had longer survival with end-stage solid tumors (39) and T_3 treatment
254 enhanced chemosensitivity (40). Following tyrosine kinase inhibitor therapy, patients
255 demonstrated improved survival with treatment of hypothyroidism (41). Agonists have
256 been developed to target tissue-specific expression of the most abundant TR isomers
257 (42). Mimetics of T_3 that selectively act as TRβ agonists have been clinically successful
258 for treatment of metabolic disorders, hyperlipidemia, hypercholesterolemia, and non-
259 alcoholic steatohepatitis without the harmful cardiovascular effects mediated by TRα
260 (16,17). Our findings demonstrate that GC-1 alone decreases the ATC aggressive
261 phenotype in transduced cells in which TRβ is re-expressed and parental cell lines with
262 diverse genetic backgrounds. These results emphasize the generalizability of GC-1 to
263 activate a TRβ tumor suppression program.

264 In ATC tumors, several genetic alterations and disrupted signaling pathways are
265 usually found. Therefore, the aim is to inhibit or disrupt multiple pathways with
266 combination therapies that block cell survival and proliferation (27,43). In this study, we
267 tested representative drugs that target the MAPK, PI3K, and cell cycle pathways to
268 assess whether GC-1 could increase their effectiveness. Since we have demonstrated
269 that activation of TRβ in ATC represses the PI3K pathway through genomic mechanisms
270 (2,29), GC-1 with either Buparlisib or Alpelisib would be suppressing PI3K activity in
271 concert. In contrast, TRβ does not directly impact MAPK through transcriptomic
272 modulation so GC-1 in combination with Sorafenib demonstrated concordant effects. In
273 all studies, GC-1 reduced the effective concentrations required to observe a reduction in
274 cell viability. One of our most intriguing observations is the impact of GC-1 alone and in

275 combination with inhibitors on cancer stem cell growth in thyrosphere formation. In all
276 ATC cell types, GC-1 alone significantly reduced thyrosphere formation. Remarkably,
277 GC-1 in combination with any of the drug treatments nearly eliminated thyrosphere
278 formation.

279 GC-1 induced re-differentiation in the SW1736 cell line in 24 hours, demonstrating
280 potent transcriptional reprogramming. While we have previously demonstrated the
281 potential for TRβ to promote a more differentiated phenotype in ATC cells, this is the first
282 time we have observed the profound impact of GC-1 in a parental cell line with low TRβ
283 expression. Importantly, we observed a concomitant increase in NIS that led to a higher
284 intake of iodide. Since PDTC and ATC tumors often exhibit a marked decrease in NIS
285 expression and resistance to RAI therapy, the results presented here raise a provocative
286 implication for the use of GC-1 in combination with RAI. Critically, we found that GC-1
287 could blunt tumor growth as effectively as Sorafenib in a xenograft study confirming the
288 observations in cell-based studies. The combination of GC-1 and Sorafenib did not further
289 reduce the tumor volume or mass over the study period. Future studies establishing the
290 pharmacodynamics of GC-1 in combination with different doses of therapeutic agents will
291 elucidate the most effective combinatorial paradigm.

292 Our findings demonstrate that selective activation of TRβ with GC-1 can reduce
293 the aggressive phenotype, reduce the cancer stemness in ATC cells, increase the
294 sensitivity of these cells to therapeutic agents, and promote re-differentiation and iodide
295 uptake. Moreover, GC-1 treatment is as effective as the therapeutic Sorafenib in inhibiting
296 tumor growth. These studies provide the foundation for further investigation of the broad
297 impact of GC-1 on mitigating tumor progression, toxicity, and development of resistance

298 to treatment.

299 **MATERIALS AND METHODS**

300 **Culture of thyroid cell lines.** Anaplastic thyroid cancer cell lines (SW1736, 8505C,
301 OCUT-2, and KTC-2) and the normal-like thyroid cell line Nthy-ORI were cultured in RPMI
302 1640 growth media with L-glutamine (300 mg/L), sodium pyruvate and nonessential
303 amino acids (1%) (Corning), supplemented with 10% fetal bovine serum (Peak Serum)
304 and penicillin-streptomycin (200 IU/L) (Corning) at 37°C, 5% CO_2, and 100% humidity.
305 SW1736-EV and SW-TRβ cells were modified by lentiviral transduction as recently
306 described (10). SW1736, KTC-2, and Nthy-ORI were authenticated by the Vermont
307 Integrative Genomics Resource at the University of Vermont using short tandem repeat
308 profiles (SW1736, May 2019; KTC-2, October 2019; Nthy-ORI, August 2020). 8505C and
309 OCUT2 were authenticated by the University of Colorado using short tandem repeat
310 profiles (8505C, June 2013; OCUT-2, June 2018).

311 **Pharmacological agents.** T_3 and GC-1 (Sigma-Aldrich) were suspended in 1 M NaOH
312 (T_3) and 100% ethanol (GC-1) for stock concentrations of 1 mM before further dilution in
313 culture medium. Buparlisib, Sorafenib, Palbociclib, and Alpelisib (MedChemExpress)
314 were suspended in 100% DMSO for stock concentrations of 50-150 mM before further
315 dilution in culture medium.

316 **Cell Growth and Viability Assays.** Cell growth was measured by cell counting at
317 discrete time points. Cells were seeded in 12- well plates, then treated with GC-1,
318 Buparlisib, Alpelisib, Palbociclib, or Sorafenib to establish time and concentration effects
319 of therapeutics on cell growth. Cell viability was determined by a Sulforhodamine B assay

320 (Abcam) following the manufacturer's protocol. In brief, ATC cells were plated in 96-well
321 clear flat-bottom plates at a density of 5,000 cells per well. Cells were fixed, stained, and
322 imaged using a plate reader according to manufacturer's instructions.

323 **Migration Assay.** Cell migration was determined by wound healing assay as previously
324 described (10, 18). Media was supplemented with GC-1 (10 nM) with and without 0.5 μM
325 Buparlisib, 0.5 μM Alpelisib, 1 nM Palbociclib, or 5 μM Sorafenib. Images were obtained
326 at 0, 16, 24, 48, and 72 hours or until 100% wound closure, depending on the cell line.
327 Percent closure was calculated relative to the area of the initial scratch.

328 **Tumorsphere Assay.** Tumorspheres formed from ATC cells were used to assess self-
329 renewal and sphere-forming efficiency as previously described (10). Where indicated,
330 adherent cells were treated with 0.5 μM Buparlisib, 0.5 μM Alpelisib, 1 nM Palbociclib, 5
331 μM Sorafenib, or vehicle for 72 hours prior to tumorsphere-forming assay. Tumorspheres
332 were then cultured in with or without GC-1 (10 nM) to evaluate the effects of liganded TRβ
333 on thyrosphere growth alone or after treatment with a therapeutic agent.

334 **Western blot Analysis.** Proteins were isolated from whole cells in lysis buffer and
335 visualized by Western blot as previously described (9, 10, 18). Specific proteins were
336 detected with the indicated antibodies (Table 1); immunoreactive proteins were detected
337 by enhanced chemiluminescence (Thermo Fisher Scientific) on a ChemiDoc XRS+ (Bio-
338 Rad Laboratories).

339 **RNA Extraction and Quantitative Real-Time PCR (qRT-PCR).** Total RNA was
340 extracted using RNeasy Plus Kit (Qiagen) according to manufacturer's protocol. cDNA

341 was generated using 5X LunaScript RT SuperMix, and mRNA expression was quantified
342 by qRT-PCR using 2X Luna Universal qPCR Master Mix (New England Biolabs) on a
343 QuantStudio 3 real-time PCR system (Applied Biosystems). Fold change in gene
344 expression compared to housekeeping controls was calculated using the ddCT method.
345 Primer sequences are indicated in Table 2.

346 **Iodide Uptake Assay.** Cells were seeded at a density of 40,000 cells per well in a 96 well
347 plate with or without 10 nM GC-1 for 48 hours. Media was discarded, and cells were
348 washed four times with warm PBS before incubation with 1 μM potassium iodide (KI,
349 Sigma-Aldrich) in PBS for 1 hour at 37°C. Wells were washed an additional four times
350 with warm PBS and 100 μL of ddH_2O were added to each well. 100 μl of 24 mM
351 ammonium cerium (IV) sulfate hydrate with 5.7% concentrated H_2SO_4 (Sigma-Aldrich)
352 and 100 μl of 24 mM sodium arsenite (III) with 205 mM sodium chloride (NaCl) and 50
353 mM sodium hydroxide (NaOH, Sigma-Aldrich) were added to each well. Plates were
354 incubated in the dark at room temperature for 30 minutes, and absorbance at 415 nm
355 was measured with a Synergy 2 Multi-Detection Microplate Reader (Agilent
356 Technologies).

357 ***In Vivo* Evaluation of Sobetirome (GC-1) and Sorafenib. T**he xenograft experiment
358 was approved by the Animal Care and Use Committee of the University of Vermont
359 (Protocol X0-018). Four-week-old athymic female nude mice (outbred homozygous nude
360 *Foxn1*^{nu}/*Foxn1*^{nu}) were purchased from Jackson Laboratory (Bar Harbor, ME, USA) and
361 were allowed to acclimatize for one week. Mice were given food and water *ad libitum*.
362 Mice were anesthetized using 3% isoflurane delivered at 1.5 L/min, and tumors were

363 established by subcutaneously injecting 1 x 10^6 8505C cells with a 26G needle in 100 μL
364 of high concentration Matrigel (Corning Inc.) diluted 1:2 with base RPMI-1640 into each
365 flank of 24 mice. One week later, mice were sorted into four treatment groups to achieve
366 approximately equal body weights within each group. Mice were then administered 0.3
367 mg/kg GC-1, 10 mg/kg Sorafenib, both GC-1 and Sorafenib, or vehicle control every day
368 via intraperitoneal injection using 27G needles. Pharmacological agents were dissolved
369 in 100% DMSO and diluted daily in 30% DMSO, 40% PEG300, and 30% PBS and
370 incubated at 55°C for 10 minutes prior to vortexing to encourage complete solubilization.
371 Tumor dimensions were measured with digital calipers, and the volumes were calculated
372 by the following formula: $(\Pi \times a \times b^2) / 6$, where a represents the largest diameter and b
373 is the perpendicular diameter. The body weight of each animal was taken at least twice a
374 week to measure toxicity. After treatment for 16 days, mice were euthanized with carbon
375 dioxide, and the tumors were harvested, fixed with formalin (Thermo Fisher Scientific),
376 and stored at 4°C prior to slide sectioning and immunohistochemistry.

377 **Immunofluorescent Analysis of Tumor Tissues.** Formalin fixed paraffin embedded
378 human thyroid xenograft tumor blocks were sectioned at 5 μm thickness onto glass
379 microscope slides, dried overnight, and then baked at 60°C for one hour. Sections were
380 deparaffinized in three changes of xylene for 15 minutes each, then dehydrated in a series
381 of graded ethanols (100% x2, 95% x2, 70%, 50%, water) for 5 minutes each. Antigen
382 retrieval utilizing 1X DAKO target Retrieval Solution (DAKO product #S1699, lot#
383 11270951; Agilent Technologies, Santa Clara, CA) in 50% glycerol was performed in a
384 Decloaking Chamber (SP1 - 100°C for 15 min, SP2 - 90°C for 1 min). Following antigen
385 retrieval, slides were cooled to room temperature in the antigen retrieval solution for 20

386 minutes. Slides were then rinsed 2x 5 minutes in distilled water followed by 0.2% Tween-
387 20 for an additional 5 minutes. Tissue sections were blocked for non-specific antibody
388 reactivity by incubation with 10% normal goat serum diluted in phosphate buffered saline
389 (PBS)/ 3% bovine serum albumin (BSA)/ 0.3% Triton X-100 for 60 minutes at room
390 temperature. Immediately following blocking, slides were incubated with rabbit polyclonal
391 anti-KI-67 (Abcam, Cambridge, UK; #ab15580) at a concentration 1.4 µg/ml in PBS/3.0%
392 BSA/0.3% Triton X-100 overnight at 4°C. Slides were then rinsed 7x 5 minutes in
393 PBS/3.0% BSA and incubated with goat anti-rabbit Alexa 488 conjugated secondary
394 antibody (ThermoFisher, Waltham MA; #A11008) in PBS/3.0% BSA for 60 minutes at
395 room temperature. Staining was followed by 5x 5 minute rinses with PBS/3.0% BSA.
396 Samples were counterstained with 4', 6-diamidino-2-phenylindole (DAPI) (ThermoFisher,
397 #D1306) at a concentration of 10 µg/ml in PBS / 3.0%BSA for 15 minutes then rinsed 3x
398 5 minutes in distilled water. Following rinses slides were mounted with a #1.5 coverslip
399 and DAKO IF mounting media (Agilent; #S3023) for imaging.

400 **Confocal Imaging of human thyroid xenograft tissue.** Xenograft samples stained with
401 anti-KI-67 and DAPI were imaged on a Nikon A1R HD point scanning confocal
402 microscope with a 20x Plan Apo λ DIC objective lens (NA 0.75, WD 1000 µm) with 488
403 nm and 405 nm laser excitation respectively. Image acquisition was completed in
404 galvanometic scanning mode (Nikon Instruments Inc., Melville NY). Images of the entire
405 xenograft section were acquired at 12-bit resolution using the tile scan function. Images
406 were saved in ND2 file format in NIS Elements (version 5.2.1, Nikon, Tokyo, Japan).

407 **Indica Labs HALO Image Analysis.** Images were analyzed using HALO image analysis
408 (Indica Labs, Albuquerque NM; version 3.3.45) utilizing the HighPlex FL module (version

409 4.1.3). Regions of interest containing only tumor tissue were outlined on each tiled
410 image. Nuclear detection was set to the DAPI channel and the nuclear detection settings
411 were optimized to accurately segment nuclei in the images. Membrane and cytoplasmic
412 threshold settings were optimized for Ki-67 staining in the Alexa 488 (green) channel.
413 Cytoplasmic detection settings were set to 4095 (in a 12 bit image) so that no cytoplasmic
414 background staining would be included in the analysis. Nuclear positive signal setting
415 threshold was set per image, to most accurately reflect the antibody staining level
416 observed in the image. Percent Ki-67 positive cells were summarized.

417 **Ethics statement and animal modeling.** All animal procedures were approved by
418 Institutional Animal Care and Use Committee (IACUC) at the University of Vermont. All
419 animals were maintained in pathogen-free conditions and cared for in accordance with
420 IACUC policies and certification. All surgeries were performed with isoflurane anesthesia.
421 Temperature-controlled post-surgical monitoring was implemented to minimize suffering.
422 Mice carrying anaplastic thyroid tumors were euthanized at designated time points for
423 tumor collection. We used signs of ulceration or a maximum individual tumor size of 2000
424 mm^3 as a protocol-enforced endpoint.

425 **Statistics.** All statistical analyses were performed using GraphPad Prism 9.3.1 and
426 assumed that variance was similar between experimental groups. Sample sizes were a
427 minimum of three independent experiments. Paired comparisons were conducted by
428 unpaired Student's t-test assuming two-tailed distribution. Group comparisons were made
429 by one-way ANOVA followed by Sidak's or Tukey's multiple comparison test as
430 appropriate. Two-way ANOVA followed by a Tukey's multiple comparison test was

431 conducted for multigroup analysis. Data are represented as mean ± standard deviation
432 or standard error of the mean where indicated. Differences were considered statistically
433 significant at $p \leq 0.05$ (*$p \leq 0.05$, **$p \leq 0.01$, ***$p \leq 0.001$). Area under the curve (AUC) at
434 the 95th confidence interval was used to evaluate statistical differences in growth and
435 migration assays.

436 **ACKNOWLEDGEMENTS:**

437 The research reported here was supported by grants from National Institutes of Health
438 U54 GM115516 for the Northern New England Clinical and Translational Research
439 Network; National Cancer Institute 1F99CA245796-01; UVM Cancer Center-Lake
440 Champlain Cancer Research Organization (C3) 12577-21; and UVM Larner College of
441 Medicine. SW1736 and KTC-2 cell lines were generously provided by Dr. John Copland
442 III (Mayo Clinic). Human cell line authentication, NextGen sequencing, automated DNA
443 sequencing and molecular imaging was performed in the Vermont Integrative Genomics
444 Resource supported by the University of Vermont Cancer Center, Lake Champlain
445 Cancer Research Organization, and the UVM Larner College of Medicine. Additional
446 human cell lines 8505C and OCUT-2 were obtained and authenticated from the University
447 of Colordo Cancer Center Tissue Culture Shared Resource supported by National Cancer
448 Institute P30CA046934. Immunofluorescence staining, imaging and analysis was
449 performed at the Microscopy Imaging Center at the University of Vermont (RRID#
450 SCR_018821). Confocal microscopy was performed on a Nikon A1R-HD point scanning
451 confocal microscope supported by NIH award number 1S10OD025030-01 from the Office
452 of Research Infrastructure Programs. We thank the Histology Research Support Facility
453 for histological services in the Department of Pathology and Laboratory Medicine at the

University of Vermont Medical Center, Burlington, VT. We thank the Office of Animal Care Management for their expertise for *in vivo* experiments.

Authors' Contribution Statement: NEG: Conceptualization, Formal analysis, Investigation, Writing – Review & editing. **LMC:** Formal analysis, Investigation, Writing. **ERW:** Formal analysis, Investigation. **CDD**: Formal analysis, Investigation. **JAT:** Investigation, Writing – Review & editing. **ELB:** Conceptualization, – Review & editing. **FEC:** Conceptualization, Resources, Writing-Review & editing, Supervision, Project administration, Funding acquisition.

Authors' Disclosure Statement: The authors declare they have no conflict of interest.

Funding Statement: The research reported here was supported by grants from National Institutes of Health U54 GM115516 for the Northern New England Clinical and Translational Research Network; National Cancer Institute 1F99CA245796-01; UVM Cancer Center-Lake Champlain Cancer Research Organization (C3) 12577-21; and UVM Larner College of Medicine.

REFERENCES

1. Kim WG, Cheng SY. Thyroid hormone receptors and cancer. Biochim Biophys Acta **2013**;1830(7):3928-36 doi 10.1016/j.bbagen.2012.04.002.
2. Bolf EL, Gillis NE, Davidson CD, Rodriguez PD, Cozzens L, Tomczak JA*, et al.* Thyroid Hormone Receptor Beta Induces a Tumor-Suppressive Program in Anaplastic Thyroid Cancer. Mol Cancer Res **2020**;18(10):1443-52 doi 10.1158/1541-7786.MCR-20-0282.
3. Aranda A, Martinez-Iglesias O, Ruiz-Llorente L, Garcia-Carpizo V, Zambrano A. Thyroid receptor: roles in cancer. Trends in endocrinology and metabolism: TEM **2009**;20(7):318-24 doi 10.1016/j.tem.2009.03.011.
4. Kim WG, Zhao L, Kim DW, Willingham MC, Cheng SY. Inhibition of tumorigenesis by the thyroid hormone receptor beta in xenograft models. Thyroid **2014**;24(2):260-9 doi 10.1089/thy.2013.0054.

481 5. Kowalik MA, Puliga E, Cabras L, Sulas P, Petrelli A, Perra A*, et al.* Thyroid hormone inhibits
482 hepatocellular carcinoma progression via induction of differentiation and metabolic
483 reprogramming. J Hepatol **2020**;72(6):1159-69 doi 10.1016/j.jhep.2019.12.018.
484 6. Zhu L, Tian G, Yang Q, De G, Zhang Z, Wang Y*, et al.* Thyroid hormone receptor β1 suppresses
485 proliferation and migration by inhibiting PI3K/Akt signaling in human colorectal cancer cells.
486 Oncol Rep **2016**;36(3):1419-26 doi 10.3892/or.2016.4931.
487 7. Bolf EL, Gillis NE, Davidson CD, Cozzens LM, Kogut S, Tomczak JA*, et al.* Common tumor-
488 suppressive signaling of thyroid hormone receptor beta in breast and thyroid cancer cells. Mol
489 Carcinog **2021**;60(12):874-85 doi 10.1002/mc.23352.
490 8. López-Mateo I, Alonso-Merino E, Suarez-Cabrera C, Park JW, Cheng SY, Alemany S*, et al.* Thyroid
491 Hormone Receptor β Inhibits Self-Renewal Capacity of Breast Cancer Stem Cells. Thyroid
492 **2020**;30(1):116-32 doi 10.1089/thy.2019.0175.
493 9. Martínez-Iglesias O, Ruiz-Llorente L, Jurado CC, Aranda A. Chapter 11 - Thyroid Hormone
494 Receptors and their Role in Cell Proliferation and Cancer. In: Ulloa-Aguirre A, Tao Y-X, editors.
495 Cellular Endocrinology in Health and Disease (Second Edition). Boston: Academic Press; 2021. p
496 229-46.
497 10. Carr FE, Tai PW, Barnum MS, Gillis NE, Evans KG, Taber TH*, et al.* Thyroid Hormone Receptor-
498 beta (TRbeta) Mediates Runt-Related Transcription Factor 2 (Runx2) Expression in Thyroid
499 Cancer Cells: A Novel Signaling Pathway in Thyroid Cancer. Endocrinology **2016**;157(8):3278-92
500 doi 10.1210/en.2015-2046.
501 11. Pourvali K, Shimi G, Ghorbani A, Shakery A, Shirazi FH, Zand H. Selective thyroid hormone
502 receptor beta agonist, GC-1, is capable to reduce growth of colorectal tumor in syngeneic mouse
503 models. J Recept Signal Transduct Res **2022**:1-8 doi 10.1080/10799893.2022.2032748.
504 12. Davidson CD, Gillis NE, Carr FE. Thyroid Hormone Receptor Beta as Tumor Suppressor: Untapped
505 Potential in Treatment and Diagnostics in Solid Tumors. Cancers (Basel) **2021**;13(17) doi
506 10.3390/cancers13174254.
507 13. Lee WK, Cheng SY. Targeting transcriptional regulators for treatment of anaplastic thyroid
508 cancer. J Cancer Metastasis Treat **2021**;7 doi 10.20517/2394-4722.2021.58.
509 14. Nabhan F, Dedhia PH, Ringel MD. Thyroid cancer, recent advances in diagnosis and therapy. Int J
510 Cancer **2021**;149(5):984-92 doi 10.1002/ijc.33690.
511 15. Saponaro F, Sestito S, Runfola M, Rapposelli S, Chiellini G. Selective Thyroid Hormone Receptor-
512 Beta (TRβ) Agonists: New Perspectives for the Treatment of Metabolic and Neurodegenerative
513 Disorders. Front Med (Lausanne) **2020**;7:331 doi 10.3389/fmed.2020.00331.
514 16. Trost SU, Swanson E, Gloss B, Wang-Iverson DB, Zhang H, Volodarsky T*, et al.* The thyroid
515 hormone receptor-beta-selective agonist GC-1 differentially affects plasma lipids and cardiac
516 activity. Endocrinology **2000**;141(9):3057-64 doi 10.1210/endo.141.9.7681.
517 17. Grover GJ, Mellstrom K, Ye L, Malm J, Li YL, Bladh LG*, et al.* Selective thyroid hormone receptor-
518 beta activation: a strategy for reduction of weight, cholesterol, and lipoprotein (a) with reduced
519 cardiovascular liability. Proc Natl Acad Sci U S A **2003**;100(17):10067-72 doi
520 10.1073/pnas.1633737100.
521 18. Kelly MJ, Pietranico-Cole S, Larigan JD, Haynes NE, Reynolds CH, Scott N*, et al.* Discovery of 2-
522 [3,5-dichloro-4-(5-isopropyl-6-oxo-1,6-dihydropyridazin-3-yloxy)phenyl]-3,5-dio xo-2,3,4,5-
523 tetrahydro[1,2,4]triazine-6-carbonitrile (MGL-3196), a Highly Selective Thyroid Hormone
524 Receptor beta agonist in clinical trials for the treatment of dyslipidemia. J Med Chem
525 **2014**;57(10):3912-23 doi 10.1021/jm4019299.
526 19. Elbers LP, Kastelein JJ, Sjouke B. Thyroid Hormone Mimetics: the Past, Current Status and Future
527 Challenges. Curr Atheroscler Rep **2016**;18(3):14 doi 10.1007/s11883-016-0564-7.

528 20. Siegel RL, Miller KD, Jemal A. Cancer Statistics, 2017. CA Cancer J Clin **2017**;67(1):7-30 doi
529 10.3322/caac.21387.
530 21. Pereira M, Williams VL, Hallanger Johnson J, Valderrabano P. Thyroid Cancer Incidence Trends in
531 the United States: Association with Changes in Professional Guideline Recommendations.
532 Thyroid **2020**;30(8):1132-40 doi 10.1089/thy.2019.0415.
533 22. Glaser SM, Mandish SF, Gill BS, Balasubramani GK, Clump DA, Beriwal S. Anaplastic thyroid
534 cancer: Prognostic factors, patterns of care, and overall survival. Head Neck **2016**;38 Suppl
535 1:E2083-90 doi 10.1002/hed.24384.
536 23. Prasongsook N, Kumar A, Chintakuntlawar AV, Foote RL, Kasperbauer J, Molina J*, et al.* Survival
537 in Response to Multimodal Therapy in Anaplastic Thyroid Cancer. J Clin Endocrinol Metab
538 **2017**;102(12):4506-14 doi 10.1210/jc.2017-01180.
539 24. Subbiah V, Kreitman RJ, Wainberg ZA, Cho JY, Schellens JHM, Soria JC*, et al.* Dabrafenib and
540 Trametinib Treatment in Patients With Locally Advanced or Metastatic BRAF V600-Mutant
541 Anaplastic Thyroid Cancer. J Clin Oncol **2018**;36(1):7-13 doi 10.1200/JCO.2017.73.6785.
542 25. De Leo S, Trevisan M, Fugazzola L. Recent advances in the management of anaplastic thyroid
543 cancer. Thyroid Res **2020**;13(1):17 doi 10.1186/s13044-020-00091-w.
544 26. Gentile D, Orlandi P, Banchi M, Bocci G. Preclinical and clinical combination therapies in the
545 treatment of anaplastic thyroid cancer. Med Oncol **2020**;37(3):19 doi 10.1007/s12032-020-
546 1345-2.
547 27. Molinaro E, Romei C, Biagini A, Sabini E, Agate L, Mazzeo S*, et al.* Anaplastic thyroid carcinoma:
548 from clinicopathology to genetics and advanced therapies. Nature Reviews Endocrinology
549 **2017**;13:644 doi 10.1038/nrendo.2017.76.
550 28. Landa I, Ibrahimpasic T, Boucai L, Sinha R, Knauf JA, Shah RH*, et al.* Genomic and transcriptomic
551 hallmarks of poorly differentiated and anaplastic thyroid cancers. The Journal of Clinical
552 Investigation **2016**;126(3):1052-66 doi 10.1172/JCI85271.
553 29. Davidson CD, Bolf EL, Gillis NE, Cozzens LM, Tomczak JA, Carr FE. Thyroid hormone receptor beta
554 inhibits the PI3K-Akt-mTOR signaling axis in anaplastic thyroid cancer cell lines via genomic
555 mechanisms. Journal of the Endocrine Society **2021** doi 10.1210/jendso/bvab102.
556 30. Silva JM, Domínguez G, González-Sancho JM, García JM, Silva J, García-Andrade C*, et al.*
557 Expression of thyroid hormone receptor/erbA genes is altered in human breast cancer.
558 Oncogene **2002**;21:4307 doi 10.1038/sj.onc.1205534.
559 31. Kim W, Cheng S. Thyroid hormone receptors and cancer. Volume 1830. Biochim Biophys
560 Acta2013. p 3928-36.
561 32. Jezequel P, Campone M, Gouraud W, Guerin-Charbonnel C, Leux C, Ricolleau G*, et al.* bc-
562 GenExMiner: an easy-to-use online platform for gene prognostic analyses in breast cancer.
563 Breast Cancer Res Treat **2012**;131(3):765-75 doi 10.1007/s10549-011-1457-7.
564 33. Jezequel P, Frenel JS, Campion L, Guerin-Charbonnel C, Gouraud W, Ricolleau G*, et al.* bc-
565 GenExMiner 3.0: new mining module computes breast cancer gene expression correlation
566 analyses. Database (Oxford) **2013**;2013:bas060 doi 10.1093/database/bas060.
567 34. Wojcicka A, Piekielko–Witkowska A, Kedzierska H, Rybicka B, Poplawski P, Boguslawska J*, et al.*
568 Epigenetic Regulation of Thyroid Hormone Receptor Beta in Renal Cancer. PLOS ONE
569 **2014**;9(5):e97624 doi 10.1371/journal.pone.0097624.
570 35. Park JW, Zhao L, Willingham M, Cheng S-y. Oncogenic mutations of thyroid hormone receptor β.
571 Oncotarget **2015**;6(10):8115-31.
572 36. Kim WG, Zhu X, Kim DW, Zhang L, Kebebew E, Cheng SY. Reactivation of the silenced thyroid
573 hormone receptor beta gene expression delays thyroid tumor progression. Endocrinology
574 **2013**;154(1):25-35 doi 10.1210/en.2012-1728.

575 37. Suzuki H, Willingham MC, Cheng SY. Mice with a mutation in the thyroid hormone receptor beta
576 gene spontaneously develop thyroid carcinoma: a mouse model of thyroid carcinogenesis.
577 Thyroid **2002**;12(11):963-9 doi 10.1089/105072502320908295.
578 38. Zhu X, Zhao L, Park JW, Willingham MC, Cheng SY. Synergistic signaling of KRAS and thyroid
579 hormone receptor beta mutants promotes undifferentiated thyroid cancer through MYC up-
580 regulation. Neoplasia **2014**;16(9):757-69 doi 10.1016/j.neo.2014.08.003.
581 39. Hercbergs A, Johnson RE, Ashur-Fabian O, Garfield DH, Davis PJ. Medically induced euthyroid
582 hypothyroxinemia may extend survival in compassionate need cancer patients: an observational
583 study. Oncologist **2015**;20(1):72-6 doi 10.1634/theoncologist.2014-0308.
584 40. Huang J, Jin L, Ji G, Xing L, Xu C, Xiong X*, et al.* Implication from thyroid function decreasing
585 during chemotherapy in breast cancer patients: chemosensitization role of triiodothyronine.
586 BMC Cancer **2013**;13:334 doi 10.1186/1471-2407-13-334.
587 41. Lechner MG, Vyas CM, Hamnvik OR, Alexander EK, Larsen PR, Choueiri TK*, et al.* Hypothyroidism
588 During Tyrosine Kinase Inhibitor Therapy Is Associated with Longer Survival in Patients with
589 Advanced Nonthyroidal Cancers. Thyroid **2018**;28(4):445-53 doi 10.1089/thy.2017.0587.
590 42. Davis PJ, Tang HY, Hercbergs A, Lin HY, Keating KA, Mousa SA. Bioactivity of Thyroid Hormone
591 Analogs at Cancer Cells. Front Endocrinol (Lausanne) **2018**;9:739 doi 10.3389/fendo.2018.00739.
592 43. Alobuia W, Gillis A, Kebebew E. Contemporary Management of Anaplastic Thyroid Cancer. Curr
593 Treat Options Oncol **2020**;21(10):78 doi 10.1007/s11864-020-00776-2.

594

1 **SUPPLEMENT**

2

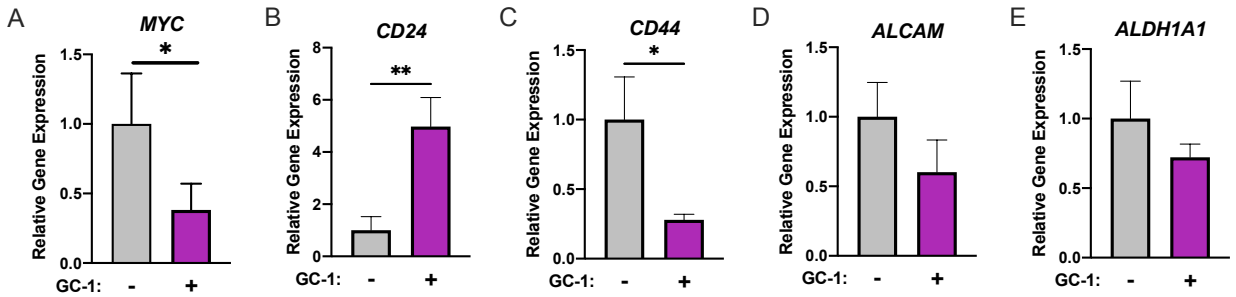

3

4 **Supplemental Figure 1.** RT-qPCR for markers of stemness and proliferation was performed on

5 SW1736 cells treated with or without 10 nM GC-1 for 24 hours. mRNA levels in cells treated

6 with GC-1 are relative to the untreated cells. Significance (* $p<0.05$) was determined by

7 Student's unpaired t test; 3 independent experiments were performed per treatment group.

8

Antibody Table

Target	Use	Antibody	Manufacturer
PARP	WB	9542	Cell Signaling Technology
Caspase-3	WB	14220	Cell Signaling Technology
Cleaved Caspase-3	WB	9664	Cell Signaling Technology
NIS	WB	MABC1191	Sigma Aldrich
GAPDH	WB	600-401-A33	Rockland Immunochemicals
Goat anti-mouse HRP	WB	7076	Cell Signaling Technology
Mouse anti-rabbit HRP	WB	211-035-109	Jackson Immunoresearch Laboratories

Isotype	Dilution	Antibody Id	MW (kDa)
rabbit	1/1,000	AB_2160739	89,116
rabbit IgG	1/500	AB_2798429	35,19,17
rabbit IgG	1/500	AB_2070042	17,19
mouse	1/500	N/A	75
rabbit	1/5,000	AB_2107593	37
goat	1/10,000	AB_330924	
mouse	1/10,000	AB_2339150	

Primer Table

Target	**Forward (5'-3')**	**Reverse (5'-3')**
ALCAM	TCAAGGTGTTCAAGCAACCA	CTGAAATGCAGTCACCCAAC
ALDH1A1	GCACGCCAGACTTACCTGTC	CCTCCTCAGTTGCAGGATTAAAG
CD24	TGAAGAACATGTGAGAGGTTTGAC	GAAAACTGAATCTCCATTCCACAA
CD44	CCAGAAGGAACAGTGGTTTGGC	ACTGTCCTCTGGGCTTGGTGTT
DIO1	CACTGCCTGAGAGGCTCTACATA	TGTAGTTCCAAGGGCCAGAT
DIO2	CCTGGTTGCAGCACATTCAC	TTGACTAGCACTGCCTCAGC
DUOX1	CCTGGCTCTAGCATGGACAC	TCCCACGAAATGGGGTTCTG
DUOX2	GCTGCCTTCCCTTAGTGAGT	TCGCTGGCACTCCATCTTTG
FOXE1	CACGGTGGACTTCTACGGG	GGACACGAACCGATCTATCCC
GAPDH	ATGTTCGTCATGGGTGTGAA	TGTGGTCATGAGTCCTTCCA
MYC	GGCTCCTGGCAAAAGGTCA	CTGCGTAGTTGTGCTGATGT
NKX2-1	CTCGCTCATTTGTTGGCGAC	GGAGTCGTGTGCTTTGGACT
PAX8	AGTCACCCCAGTCGGATTC	CTGCTCTGTGAGTCAATGCTTA
SLC5A5	GCAGTACATTGTAGCCACGAT	TGCAGATAATTCCGGTGGACA
SLC26A4	TGAAGGAAATGCCAAAGTTACG	AGTATTCCCGCAGTTTGCTGA
TG	AGGGAGAGTTTATGCCTGTCC	CAATACCCAGATACCTCAGGGAA
THRA	AGGTCACCAGATGGAAAGCG	AGTGATAACCAGTTGCCTTGTC
THRB	CACATCATCATGGTCCAGATGG	GGCGCAGCACGTTGAAAAAT
TPO	GCCAACAAGCGGAGTGATTG	GGGCAGCATGTAAGGGAGAC
TSHR	TTCCCTGACCTGACCAAAGTT	ACGTCATGTAAGGGTTGTCTGT

Amplicon Size (bp)
96
129
208
151
75
125
72
132
154
143
119
163
139
122
97
148
136
92
175
76